

Generative Head-Mounted Camera Captures for Photorealistic Avatars

SHAOJIE BAI^{1*}, SEUNGHYEON SEO^{1,2†*}, YIDA WANG¹, CHENGHUI LI¹, OWEN WANG¹, TE-LI WANG¹, TIANYANG MA¹, JASON SARAGIH¹, SHIH-EN WEI¹, NOJUN KWAK², and HYUNG JUN KIM¹,

¹Meta Reality Labs, USA ²Seoul National University, Republic of Korea

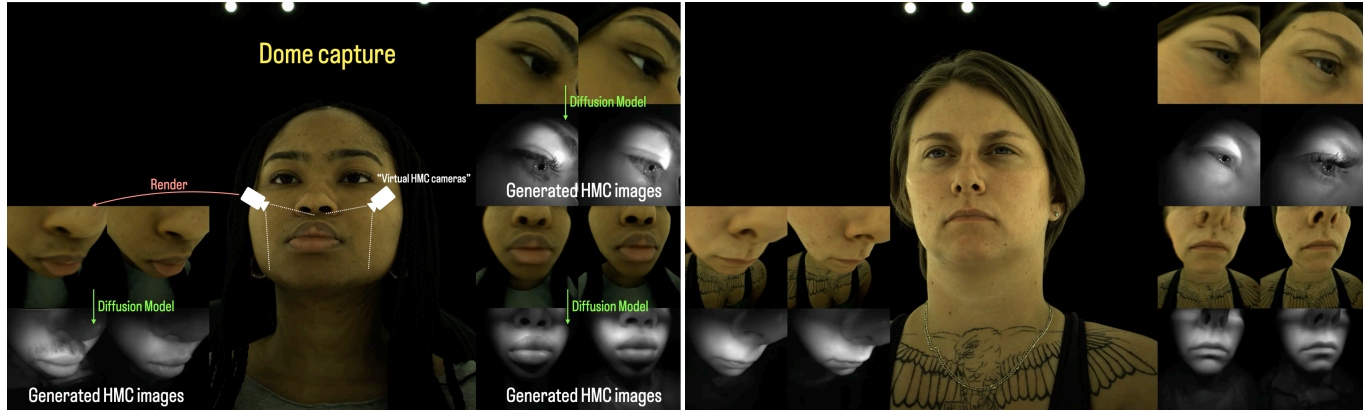


Fig. 1. GenHMC establishes an HMC-avatar correspondence *directly* via a dome capture and an image diffusion model. These “generative” captures introduce natural augmentations to identity information without altering the expressions.

Enabling photorealistic avatar animations in virtual and augmented reality (VR/AR) has been challenging because of the difficulty of obtaining ground truth state of faces. It is *physically impossible* to obtain synchronized images from head-mounted cameras (HMC) sensing input, which has partial observations in infrared (IR), and an array of outside-in dome cameras, which have full observations that match avatars’ appearance. Prior works relying on analysis-by-synthesis methods could generate accurate ground truth, but suffer from imperfect disentanglement between expression and style in their personalized training. The reliance of extensive paired captures (HMC and dome) for the *same* subject makes it operationally expensive to collect large-scale datasets, which cannot be reused for different HMC viewpoints and lighting. In this work, we propose a novel generative approach, **Generative HMC** (GenHMC), that leverages *large unpaired HMC captures*, which are much easier to collect, to directly generate high-quality *synthetic* HMC images given any conditioning avatar state from dome captures. We show that our method is able to properly disentangle the input conditioning signal that specifies facial expression and viewpoint, from facial appearance, leading to more accurate ground truth. Furthermore, our method can generalize to unseen identities, removing the reliance on the paired captures.

*Both authors contributed equally to this research.

†Work done during an internship at Meta Reality Labs.

Authors’ Contact Information: Shaojie Bai¹, shaojiebai@gmail.com; Seunghyeon Seo^{1,2}, zzzlssh@snu.ac.kr; Yida Wang¹, yidawang@meta.com; Chenghui Li¹, leochli@meta.com; Owen Wang¹, ojwang@meta.com; Te-Li Wang¹, teli@meta.com; Tianyang Ma¹, tianyang@meta.com; Jason Saragih¹, jsaragih@meta.com; Shih-En Wei¹, swei@meta.com; Nojun Kwak², nojunk@snu.ac.kr; Hyung Jun Kim¹, johnkim@meta.com, ¹Meta Reality Labs, USA and ²Seoul National University, Republic of Korea.

Conference acronym ’XX, June 03–05, 2018, Woodstock, NY

© 2018 Copyright held by the owner/author(s). Publication rights licensed to ACM. This is the author’s version of the work. It is posted here for your personal use. Not for redistribution. The definitive Version of Record was published in *Proceedings of Make sure to enter the correct conference title from your rights confirmation email (Conference acronym ’XX)*, <https://doi.org/XXXXXXXX.XXXXXXX>.

We demonstrate these breakthroughs by both evaluating synthetic HMC images and universal face encoders trained from these new HMC-avatar correspondences, which achieve better data efficiency and state-of-the-art accuracy.

1 Introduction

The emergence of Virtual Reality (VR) devices made it possible to create a system that faithfully simulates real-world human interactions. Such a system requires not just high-quality photorealistic avatars, but also the ability to animate them to emulate the *immediacy* and *fidelity* of face-to-face conversations. Recent works have made huge progress towards this goal of photorealistic telepresence [Bai et al. 2024; Wei et al. 2019].

Despite the limited coverage of head-mounted cameras (HMC) sensing input, direct regression of avatar states (*e.g.*, blendshapes or learned latent codes) from HMC images have been proven effective and efficient [Bai et al. 2024]. The core challenge lies in the establishment of abundant input-output pairs of the system, known as the HMC-avatar correspondence problem. The difficulty comes from the opaque nature of VR headsets: it is *physically impossible* to simultaneously capture full face with HMCs, which generates sensing inputs, and with an array of outside-in cameras, where images could be used to generate ground truth state of the avatar. To overcome this challenge, prior works [Schwartz et al. 2020; Wei et al. 2019] adopted analysis-by-synthesis approaches which require (1) capturing the same subject in both HMCs and in a multi-camera dome; (2) building avatars with the data including the subject; (3) training style-transfer models to bridge domain gaps in lighting direction and spectrum (*i.e.*, infrared vs. visible), and (4) fitting full avatars to partial HMC observations.

This process has several key drawbacks in terms of both operational cost and quality. On the cost side, the need for paired HMC and dome captures creates inherent limitations. When a new head-set is introduced, the dataset must be recreated from scratch rather than reusing existing dome captures. Additionally, the analysis-by-synthesis training must be redone whenever the avatar’s expression space definition is updated. On the quality side, challenges arise from imperfect disentanglement between style transfer and expressions, leading to the “cheating” effect described in [Wei et al. 2019], due to the large domain gap between HMC and dome images. Fitting a complete avatar onto partial HMC observations also requires proper regularization for unseen parts (*e.g.*, hair) to prevent out-of-distribution artifacts, which can reduce fitting accuracy. Furthermore, the precision of the process is constrained by the avatar’s expressivity range, which is assumed to encompass all facial expressions in the HMC images. Any discrepancies in appearance or shape (*e.g.*, makeup) between the dome and HMC images can lead to fitting inaccuracies.

In this work, we introduce **Generative HMC** (GenHMC), a novel solution to the HMC-avatar correspondence problem. Instead of optimizing avatar’s expression to match real HMC images, we present a method to leverage generative models to realize “the other way around”: putting virtual HMCs on avatars to synthesize HMC images, with their expression captured in dome, via diffusion models. To achieve this, we leverage a large pool of *unpaired* HMC captures (which are much easier to obtain than paired data) to build a foundational HMC image generation model. Specifically, we design and train a U-Net based diffusion model, conditioned on expression-related features, such as keypoints and segmentations, which are obtainable from both HMC images and avatar projections. With this model, we can now freely sample new HMC images from any specific avatar state captured in a dome.

Our approach effectively addresses several of these limitations. First, it significantly reduces the cost of generating HMC-avatar correspondences: our diffusion model requires training only once, and generalizes to expression features from avatars with unseen identities. This eliminates the need for paired captures, and repeated training for any updates in the avatar’s expression space, as the expression features are agnostic to latent expression values. Second, the quality of the correspondences is improved by directly using ground truth measurements from dome captures, free from out-of-distribution issues. When sampling with a certain expression captured in the dome, the model can generate diversity in the non-expression factors (*e.g.*, illumination, appearance), improving the robustness of downstream face encoder systems. Finally, with extensive experiments, we show that combining these synthetic data with conventional HMC-correspondences (from real HMC images) significantly outperforms the baseline face encoder trained solely on real data. Our contributions are summarized as follows:

- A novel approach to generate HMC-avatar correspondences by sampling from an expression-conditioned diffusion model trained from unpaired HMC captures.
- A demonstration that face encoders trained from synthetic data outperform baseline models.
- A scaling law analysis showing how GenHMC impacts the performance and efficiency of the face encoder training pipeline.

2 Related Works

2.1 Photorealistic Avatars

The pursuit of photorealistic digital avatars has become central in computer vision and graphics, driven by the demand for immersive virtual experiences. Foundational work by Blanz and Vetter [1999] introduced 3D morphable models for realistic face synthesis, followed by multi-view capture systems that improved facial geometry and appearance reconstruction [Beeler et al. 2011; Bickel et al. 2007; Bradley et al. 2010; Furukawa and Ponce 2009; Fyffe et al. 2014; Ghosh et al. 2011; Huang et al. 2006; Kludiny and Hilton 2012; Zhang et al. 2004]. Texture mapping further enhanced realism with lifelike skin detail [Debevec et al. 2000; Donner et al. 2008; Weyrich et al. 2006]. More recently, the field has shifted to learning-based methods. Building on Active Appearance Models [Cootes et al. 2001], deep learning approaches [Gecer et al. 2019; Lombardi et al. 2018; Shysheya et al. 2019] have achieved higher fidelity and expressiveness than classical techniques [Cao et al. 2016; Ichim et al. 2015; Seymour et al. 2017]. These methods support advanced capabilities like gaze control, relighting, and volumetric modeling for hair [Bi et al. 2021; Rosu et al. 2022; Schwartz et al. 2020; Yang et al. 2023], and enable realistic avatar generation from limited inputs, including handheld device captures [Cao et al. 2022; Grassal et al. 2022].

2.2 Establishing HMC-avatar Correspondences

Registering 3D face models to HMC captures is essential for accurate VR face tracking. Traditional landmark-based methods [Wei et al. 2019] yield sparse correspondences and struggle with subtle motions under oblique views. Depth sensor-based methods [Li et al. 2015; Thies et al. 2018] captured lower-face geometry more directly but required carefully positioned cameras. Some approaches relied on users mimicking predefined expressions aligned with audio, resulting in coarse, discrete tracking [Olszewski et al. 2016]. With more expressive avatars, analysis-by-synthesis methods [Nair et al. 2008] were explored, but domain gaps between avatar renderings and real HMC images remained a challenge. Wei et al. [2019] addressed this with a two-stage CycleGAN and differentiable rendering pipeline, though semantic shifts often occurred. Schwartz et al. [2020] improved on this by jointly training expression regression and style transfer, reducing domain mismatch through end-to-end learning. In this work, we leverage high-fidelity dome captures and a generative diffusion model to establish accurate, expressive HMC-avatar correspondences with far less manual effort and system complexity.

2.3 Synthetic Data Training for Neural Network

Synthetic data has become a pivotal strategy in generating large labeled datasets, enhancing vision task performance [He et al. 2023; Tian et al. 2024]. It has been widely utilized in various computer vision domains [Abu Alhaija et al. 2018; Chen et al. 2019; Fischer et al. 2015; Mayer et al. 2016; Peng et al. 2015; Ros et al. 2016], effectively addressing data scarcity and annotation costs. Recently, large-scale text-to-image models [Balaji et al. 2022; Nichol et al. 2022; Ramesh et al. 2022; Rombach et al. 2022; Saharia et al. 2022] have expanded synthetic data capabilities. Integrating such generated images with real datasets substantially improves supervised learning tasks [Azizi et al. 2023; He et al. 2023; Saryıldız et al. 2023]. Notably, synthetic

images from GLIDE [Nichol et al. 2022] enhanced zero-shot and few-shot classification [He et al. 2023], and diffusion-based augmentation improved few-shot learning [Trabucchi et al. 2023].

3 Preliminaries

3.1 Codec Avatars

A Codec Avatar, which consists of an encoder-decoder pair, denoted as $(\mathcal{E}, \mathcal{D})$, respectively, has emerged as a powerful paradigm for compactly representing and reconstructing high-fidelity facial dynamics. It aims to reduce both reconstruction error (distortion) between the original and reconstructed data, and the overall delay (latency) involved in replicating a user’s appearance and behavior at a remote location. In this paper, we use a universal facial encoder that takes image data from VR headset cameras as input and generates encodings of the user’s state in a universal latent space, which is independent of their identity [Bai et al. 2024].

The universal facial encoders are based upon the universal prior models (UPMs) for faces [Cao et al. 2022]. Its Codec Avatar framework includes an expression encoder, \mathcal{E}_{exp} and separate hypernetwork identity encoder, \mathcal{E}_{id} . \mathcal{E}_{exp} generates expression latent codes $\mathbf{z} \in \mathbb{R}^{4 \times 4 \times 16}$. This convolutional latent space ensures that each latent dimension influences specific spatial regions while maintaining semantic consistency across different identities. \mathcal{E}_{id} processes a neutral texture map \mathbf{T}_{neu} and a neutral geometry image \mathbf{G}_{neu} to generate multi-resolution bias maps Θ_{id} serving as parameters for the decoder \mathcal{D} , which reconstructs volumetric slabs \mathbf{M} and geometry \mathbf{G} based on disentangled control inputs, including viewpoint $\mathbf{v} \in \mathbb{R}^6$, gaze directions $\mathbf{g} \in \mathbb{R}^6$, and expression latent code \mathbf{z} . The final image I_{vol} is rendered by ray-marching R_{vol} . Furthermore, additional network modules are added to \mathcal{D} to estimate the texture maps \mathbf{T} for the face and eyes, allowing the final mesh I_{mesh} to be obtained using a mesh renderer R_{mesh} . Kindly refer to Bai et al. [2024] for further details.

3.2 Generative Diffusion Model

Diffusion models [Ho et al. 2020; Sohl-Dickstein et al. 2015; Song and Ermon 2019; Song et al. 2020b] have been introduced as powerful generative frameworks and are now widely used for high-quality image synthesis in computer vision. They transform data into noise via a forward process and learn to reverse it through a parameterized backward diffusion. The generation process can also be conditioned on various inputs such as text, keypoints, or class labels [Choi et al. 2021; Hertz et al. 2022; Hu 2024; Kawar et al. 2023; Rombach et al. 2022; Saharia et al. 2022; Zhang et al. 2023].

A diffusion model is trained by minimizing a variational upper bound or a simplified loss. A common practice is to predict the noise $\varepsilon \sim \mathcal{N}(\mathbf{0}, \mathbf{I})$ added at step $t \sim \mathcal{U}([0, 1])$ and the corresponding training objective is as follows:

$$\mathbb{E}_{\mathbf{x}, \varepsilon, c, t} [\|\varepsilon_{\theta}(\alpha_t \mathbf{x} + \sigma_t \varepsilon, \mathbf{c}, t) - \varepsilon\|_2^2], \quad (1)$$

where ε_{θ} and \mathbf{c} are the diffusion model (with ε -prediction) and the condition, respectively. Typically, α_t is chosen such that it gradually decreases with t , preserving less of the original signal over time, while σ_t increases with t , adding more noise. Therefore, the term $\alpha_t \mathbf{x} + \sigma_t \varepsilon$ represents the noisy version of \mathbf{x} at time t with $\alpha_t = \sqrt{\bar{\alpha}_t}$

and $\sigma_t = \sqrt{1 - \bar{\alpha}_t}$ derived from a variance schedule, where $\bar{\alpha}_t = \prod_{s=1}^t (1 - \beta_s)$ is the total noise variance. Note that β denotes the small noise variance added at each step, and kindly refer to [Ho et al. 2020] for more details.

Furthermore, a number of sampling strategies have been actively explored recently [Ho et al. 2020; Liu et al. 2022; Lu et al. 2022; Phillips et al. 2024; Song et al. 2020a; Watson et al. 2022]. Among them, DDPM [Ho et al. 2020] and DDIM [Song et al. 2020a] both begin by drawing a sample from pure noise, $\varepsilon_T \sim \mathcal{N}(\mathbf{0}, \mathbf{I})$, and iteratively produce a sequence of points, $\varepsilon_T, \varepsilon_{T-1}, \dots, \varepsilon_1$, whose level of noise is gradually reduced throughout T iterations.

Classifier guidance [Dhariwal and Nichol 2021] uses gradients from a pre-trained model to boost sample quality in conditional diffusion models with reducing diversity. Classifier-free guidance [Ho and Salimans 2022], on the other hand, avoids relying on a separate pre-trained model. Instead, it trains a single diffusion model for both conditional and unconditional objectives by randomly dropping the condition c during the training phase. When sampling, it adjusts the predicted noise as follows:

$$\tilde{\varepsilon}_{\theta}(\varepsilon_t, \mathbf{c}, t) = w\varepsilon_{\theta}(\varepsilon_t, \mathbf{c}, t) + (1 - w)\varepsilon_{\theta}(\varepsilon_t, t) \quad (2)$$

where $\varepsilon_{\theta}(\varepsilon_t, \mathbf{c}, t)$, $\varepsilon_{\theta}(\varepsilon_t, t)$, and w denotes the conditional and unconditional ε -predictions, and guidance weight, respectively. Setting $w > 1$ strengthens its influence, whereas $w = 1$ effectively disables classifier-free guidance.

4 Method

In this work, we propose GenHMC, a conditional diffusion framework that generates synthetic HMC captures using a combination of keypoint and segmentation, which we have named keyseg map, as the input condition. This approach facilitates the straightforward establishment of correspondences between HMC and avatars using dome capture images (Sec. 4.1). Moreover, it enables the generation of synthetic images with diverse natural augmentations for a single expression, enhancing both flexibility and usability. Finally, we establish a system using the generative HMC captures created by GenHMC for universal facial encoder training, significantly improving the efficiency of data collection (Sec. 4.2). We also explore various applications of the proposed method, e.g., adapting to multi-view diffusion framework, light control, and glasses generation. Kindly refer to our supplementary material for the related sections.

4.1 HMC Diffusion

An overview of the general GenHMC architecture is presented in Fig. 2. During training, we load a real, monochrome HMC image $\mathbf{x} \in \mathbb{R}^{256 \times 256}$, and apply it through a pre-trained face keypoint detection model ϕ_{kpt} and a face segmentation model ϕ_{seg} . Specifically, the keypoint model detects for the upper and lower face, respectively:

- eyebrows, outer/inner eyelids, and pupil center;
 - upper/lower vermilion border, cupid’s bow, upper/lower lip, left/right lateral commissure, left/right nostril, nasal base, nose tip, tongue tip, and the top/bottom of the chin,
- each part with a different keypoint color. Likewise, the segmentation model detects for the upper and lower face, respectively:
- face region, eyeball, iris and pupil;
 - face region, upper/lower lips, inner mouth, and tongue,

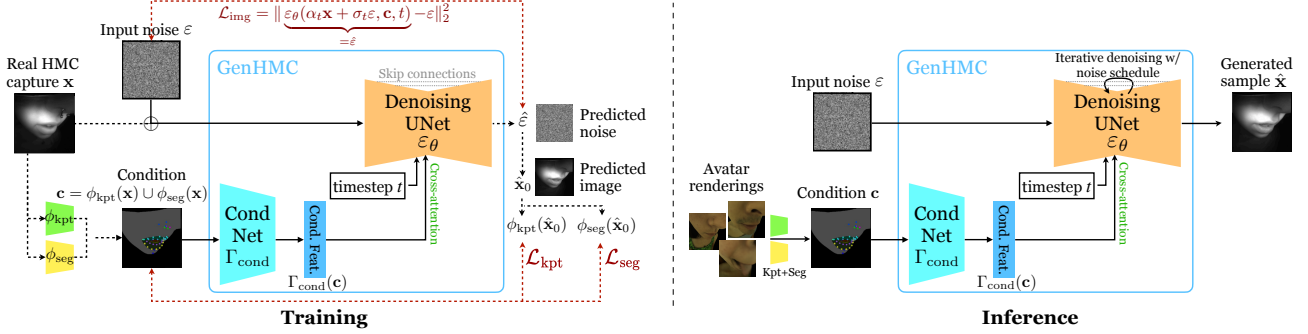


Fig. 2. **The training and inference processes of our GenHMC model.** (Left) During the training phase, we use the detected keypoint+segmentation annotations as the conditional signals, and self-supervise a conditional diffusion model training with the noise prediction loss as well as the perceptual losses. (Right) At inference time, we obtain the keypoint+segmentation conditional as the (base) control signal for expressions, and sample the diffusion model to generate high-quality synthetic HMC data that aligns with this expression.

each part with a different segmentation class color. We then overlay the detected results of the two models on the same image c :

$$c = c_{\text{keyseg}} = \phi_{\text{kpt}}(x) \cup \phi_{\text{seg}}(x) \quad (3)$$

which we then use as the conditional signal for the generative model. Meanwhile, we randomly sample a Gaussian noise $\varepsilon \sim \mathcal{N}(0, I) \in \mathbb{R}^{256 \times 256}$, and timestep $t \in \mathcal{U}([0, 1])$, and diffuse the original image x by $\tilde{x}_t = \alpha_t x + \sigma_t \varepsilon$ (following the notation of Eq.(1); see Ho et al. [2020] for more details).

To train the diffusion model, we pass the conditional c through a shallow convolutional network Γ_{cond} , which is based on MobileNetV3 [Howard et al. 2019], to obtain a lower-resolution feature map $\Gamma_{\text{cond}}(c) \in \mathbb{R}^{C \times 12 \times 12}$ where C is the feature dimension (in practice, we set $C = 160$, following the output dimension of MobileNetV3). This conditional feature map is then flattened and injected into the bottleneck of the denoising U-Net (see **orange** module in Fig. 2) via a cross-attention layer. With the conditional feature map, the diffused image \tilde{x}_t and the timestep t , the denoising U-Net then tries to predict the noise $\hat{\varepsilon} = \varepsilon_\theta(\tilde{x}_t, c, t)$ and an posterior estimate of the reconstructed image \hat{x}_0 .

We propose three training objectives. First, following prior works on diffusion models [Ho et al. 2020; Song et al. 2020b], the reconstruction loss on noise:

$$\mathcal{L}_{\text{img}} = \|\varepsilon_\theta(\alpha_t x + \sigma_t \varepsilon, c, t) - \varepsilon\|_2^2 \quad (4)$$

We also found it beneficial to add the perceptual losses which compares the originally detected keypoint heatmap activations, $\text{hm}(\phi_{\text{kpt}}(x))$, with that of the reconstructed posterior, $\text{hm}(\phi_{\text{kpt}}(\hat{x}_0))$,

$$\mathcal{L}_{\text{kpt}} = \|\text{hm}(\phi_{\text{kpt}}(x)) - \text{hm}(\phi_{\text{kpt}}(\hat{x}_0))\|_2^2 \quad (5)$$

and corresponding segmentation maps with a pixel-wise cross-entropy loss,

$$\mathcal{L}_{\text{seg}} = \text{CrossEntropy}(\text{logit}(\phi_{\text{seg}}(\hat{x}_0)), \phi_{\text{seg}}(x)), \quad (6)$$

where $\text{logit}(\cdot)$ represents the pre-softmax logits for the segmentation map. In summary, the total loss is a weighted combination of these three losses with the balancing weights λ s:

$$\mathcal{L}_{\text{total}} = \lambda_{\text{img}} \mathcal{L}_{\text{img}} + \lambda_{\text{kpt}} \mathcal{L}_{\text{kpt}} + \lambda_{\text{seg}} \mathcal{L}_{\text{seg}}. \quad (7)$$

At inference time, no real HMC image is available (after all, we are to generate them). We instead take the avatar renderings from

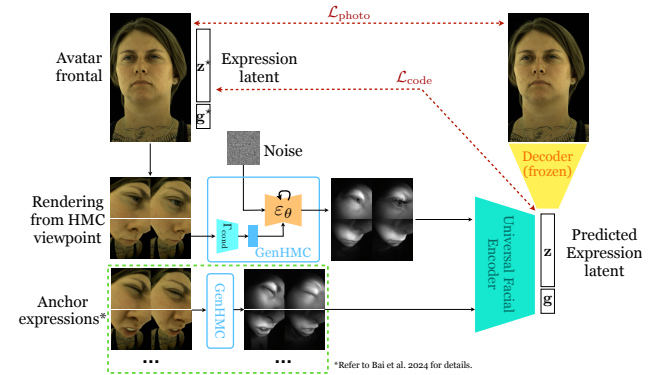


Fig. 3. **Directly training universal facial encoder with GenHMC-based HMC-avatar correspondences.** Using the GenHMC approach, we can directly establish HMC-avatar correspondences and train on *dome capture frames*. This is vastly different from the traditional approach which requires an HMC capture paired with the dome capture of the subject.

simulated HMC viewpoints, detect/project the keypoint and segmentation maps on them, and use the outcome as conditional c . In the meantime, we sample $\varepsilon \sim \mathcal{N}(0, I)$ and iteratively denoise it with ε_θ following a sampling schedule (DDPM [Ho et al. 2020], DDIM [Song et al. 2020a], etc.) from $t = 1$ to $t = 0$ with the conditional c .

Discussions. We note that this flow falls into a broader category of works which employ conditional generative models as unsupervised priors to resolve *inverse problems* [Daras et al. 2024; Song et al. 2021], where the generative model aims to reconstruct a full observation from a partial measurement (in our case, keypoint+segmentation maps c representing the expression). We also specifically did not use the latent diffusion model (LDM) [Rombach et al. 2022] as it entails a separate VAE training process, and in this case we only need a relatively lightweight 256×256 monochrome image.

4.2 Encoder Training

As illustrated in Fig. 3, we present a novel encoder training system that minimizes the need for real HMC captures. The training system comprises two major components: GenHMC inference as illustrated in Fig. 2, and the encoder training with therefore synchronized dome assets. For the first time, dome assets, such as ground truth

expression codes, or even dome images can be directly utilized to train face encoders for VR headsets. This approach offers several key benefits: (1) more accurate ground truth supervision from multi-view dome captures, comparing against pseudo correspondences established by [Wei et al. 2019], (2) reduced need for paired HMC and dome captures, and (3) increased diversity in HMC inputs resulted from GenHMC.

We follow the exact setup of Bai et al. [2024] for the state-of-the-art universal facial encoder model architecture, and refer interested readers to it for more details.

5 Experiments

In this section, we demonstrate the quantitative and qualitative results of the GenHMC method. In Sec. 5.1, we start by describing the datasets we use as well as the baseline approaches for establishing and training with the HMC-avatar correspondences. Then in Sec. 5.2, we delve into analysis of the scalability of GenHMC generative model, and study a key downstream application of the GenHMC framework by building a universal facial encoder system with the synthetic captures and comparing with the baseline method.

5.1 Experimental Details

5.1.1 Datasets. The datasets we use in this section consist of four different categories.

Avatar dome captures. We captured 341 subjects’ multi-view face performances in a spherical capture dome equipped with 90 colored/monochrome high-resolution cameras. Specifically, we follow the setup of Cao et al. [2022], where each subject is asked to perform 20 minutes of facial expressions, neutral and emotional speeches, head movements, and gaze sequences. The visual data are captured with relighting at 30 FPS and resolution 4096×2668 , which is more than 12M frames in total. Subsequently, we use them to train a relightable universal Gaussian Codec Avatar model [Li et al. 2024] (*i.e.*, the *decoder*) for the 341 subjects.

Paired (with dome capture) HMC captures. For each of these 341 subjects, we also collect the head-mounted camera (HMC) captures of these very same subjects, on the same day, with a modified version of the Quest Pro VR headset that contains augmented training cameras which provide better lower-face visibility (we refer interested readers to Fig. 2 of Bai et al. [2024] for more details). Each subject is asked to perform roughly 9 minutes of range of facial motions, speeches, as well as gaze sequences, while changing the headset donning after every few capture segments. The HMC images are captured at 72 FPS with resolution 400×400 , but we downsample the images to 192×192 for universal facial encoder training. This dataset consists entirely of *real* HMC data, and we follow Wei et al. [2019]’s personalized style-transfer approach, which requires the augmented camera images, to generate the corresponding expression latent codes using the decoder.

Unpaired large-scale HMC captures. We also leverage a large pool of HMC captures of over 17K subjects. The capture script is the same as the HMC captures above (roughly 40K frames per subject), except that none of these subjects has a corresponding dome capture (*i.e.*, we don’t have their avatars). This dataset is primarily used to train our GenHMC model.

Synthetic HMC captures. For each dome capture frame of every subject, we render the photorealistic avatar from an HMC-alike camera view (with simulated distortions) and apply the GenHMC approach to generate the corresponding monochrome, infrared-spectrum synthetic HMC images following the process of Fig. 2. Therefore, these synthetic HMC captures have the same frame rate, frame count, and “capture script” as the aforementioned dome captures, totaling over 12M frames.

5.1.2 Baselines. Our method introduces a novel formulation for generating HMC-avatar correspondences. As the first generative approach that enables this, GenHMC allows many new functionalities and capabilities that had not existed in prior works, which we elaborate on in Sec. 5.2.

Meanwhile, we demonstrate the benefits of our approach by comparing the universal facial encoder trained using our GenHMC data, with the encoder trained using only real HMC data and the *best* existing approach that builds pseudo HMC-avatar correspondences, requiring operationally costly paired dome & HMC captures, augmented headset cameras, and person-specific style-transfer modules [Wei et al. 2019]. Unless otherwise noted, all encoders are initialized with pre-trained weights from the self-supervised learning framework proposed by Bai et al. [2024], which currently represents the state-of-the-art in encoder training, achieving the best generalization error on unseen identities.

5.1.3 Evaluation Metrics. To properly evaluate the universal facial encoder’s generalizations, we keep a held-out set of 34 test subjects (out of 341) whose neither 3D avatar models nor HMC images are available during encoder training. We train on the rest 307 subjects’ real HMC data and/or GenHMC data (generated from their avatars), and evaluate the trained encoders on this held-out test set to assess the model’s ability to generalize to unseen subjects.

Following Bai et al. [2024], we primarily compute the following set of metrics:

- **Photometric Image L_1 Error.** Pixel-level errors of the renderings of the encoder-predicted expression on the avatar.
- **Geometric L_2 error.** L_2 displacement error of the encoder-predicted vs. ground truth face mesh, measured in millimeters (mm) and averaged over all facial region vertices.
- **Geometric L_2 error on mouth region.** Similar as the geometric L_2 error above, but only on the mouth (and surrounding) region vertices.
- **Lip shape error.** The average of the horizontal (distance between left and right lip corners) and vertical (distance between center upper and lower lips) lip shape errors, which is especially important for speech.

Importantly, we note that throughout this section, the so-called “ground truth” expressions of the real HMC captures are not the true actual ground truth (which is impossible to obtain), but instead from the style-transfer based HMC-avatar correspondences generated by the method of Wei et al. [2019]. **It is therefore a biased estimation that is subject to errors still, but nevertheless a consistent reference in an ablative setting**, aligning with the prior works’ convention [Bai et al. 2024; Chen et al. 2021; Martinez et al. 2024; Schwartz et al. 2020].

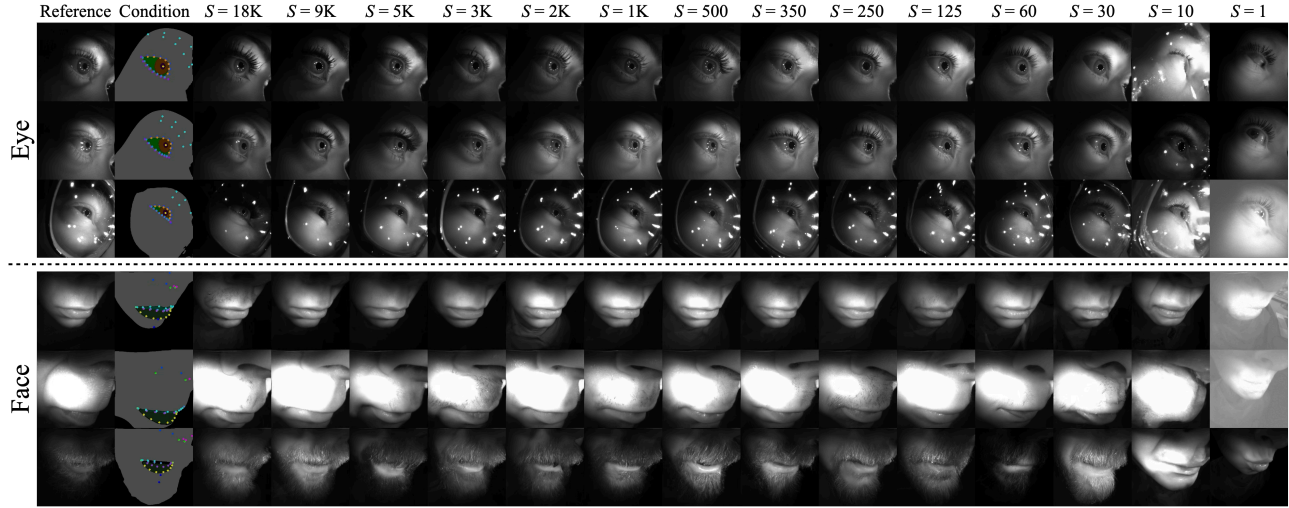


Fig. 4. **Effect of training size on GenHMC inference results.** When the number of training subjects is small, the diversity of the generated output decreases, which can lead to degenerate results when an arbitrary keyseg map is provided as a condition. S denotes the training dataset size, *i.e.*, the number of training subjects.

5.2 Scalability of GenHMC

To assess the impact of training data size on GenHMC’s performance, we perform ablation studies by training models using subsets of the full dataset (18K subjects) with varying numbers of subjects (9K, 5K, 3K, and so on). As expected, we observe that reducing the number of training subjects leads to a decrease in the quality and diversity of the generated images, as shown in Fig. 4. Specifically, the inference results become increasingly degenerate, and the pixel-wise alignment between the generated outcome and the keypoint/segmentation maps degrades. In the extreme case where we train with only one subject, the model tends to generate images that closely resemble the attributes of that specific subject, indicating a significant loss of diversity. These ablation studies demonstrate the importance of a sufficiently large and diverse unpaired dataset for GenHMC to generate high-quality and diverse images, although we note that comparable results can be achieved with datasets of an order of magnitude smaller than our full 18K subject dataset. Fig. 8 demonstrates the qualitative results generated from GenHMC trained with 18K full data.

5.3 Universal Facial Encoders with GenHMC Data

A key downstream application of GenHMC is to provide synchronized dome-HMC correspondences for training universal encoder (UE). As Bai et al. [2024] noted, a major challenge is generalization, *i.e.*, models trained on limited paired data tend to overfit to the small set of training subjects.

In contrast, with GenHMC, the generative model offers natural augmentations on various axes: the GenHMC framework enables us to keep the expressions intact while varying orthogonal factors like illuminations, mustache, thickness of the eyebrow, iris color, glasses, etc. in a *controlled* manner. Indeed, we demonstrate that leveraging the GenHMC captures (in addition to some real captures) significantly improve the performance of the current best encoder

Table 1. **Quantitative comparison between UEs.** All models are trained for 200K iterations with a batch size of 16. Note that the encoder trained solely on GenHMC data performs poorly because it computes metrics against the pseudo correspondences from Wei et al. [2019], which biases towards real HMC captures. See Sec. 5.3.1 for more details.

	Photo. L_1 ↓	Geo. L_2 ↓	Geo. L_2 (Mouth) ↓	Lip Shape ↓
Real+GenHMC (Ours)	2.8598	1.2325	1.8959	1.9968
Real (Baseline)	2.9149	1.2603	1.9666	2.0921
Real w/o SSL	2.9578	1.2740	1.9811	2.1519
GenHMC Only	3.5501	1.5118	2.4387	2.5563

on held-out validation subjects on metrics across the board, offering substantially more accurate, generalizable and robust facial encoding on unseen test subjects compared to baseline. Furthermore, it leads to improved scalability with respect to the number of captures. We highlight these advantages through the following experiments. In Sec. 5.3.1, we present quantitative and qualitative studies against the baseline approach. In Sec. 5.3.2 and Sec. 5.3.3, we revisit how UE training scales when synthetic data is incorporated.

5.3.1 Comparisons with the Traditional Approach. We conducted quantitative and qualitative studies to compare facial encoders trained with real data and/or GenHMC synthetic data under 3 configurations: (1) mixing (roughly) 50% real and 50% synthetic HMC frames, (2) synthetic frames only, and (3) real frames only.

As shown in the quantitative results of Tab. 1, we show that the addition of GenHMC synthetic captures improves the robustness and generalization of the facial encoder while evaluated on held-out unseen test subjects’ data across all metrics. Notably, we improve over the current best model by over 5% on key metrics like the mouth geometry error and the lip shape error. We also specifically note that the encoder trained with synthetic captures only has a significantly higher error, which should be taken with a grain of salt. These errors are computed against the “ground truths” which

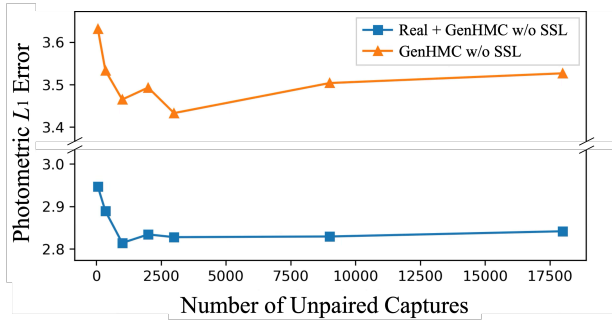


Fig. 5. **Scalability of GenHMC subjects on UE training.** Generally, the more the GenHMC training subjects there are, the more accurate the pixel-level reconstruction quality becomes during downstream UE training. We use all 307 real subjects together for training and evaluate on held-out 34 subjects. To assess the impact of GenHMC data size alone without other priors, we compare encoders trained from scratch without SSL pre-training.

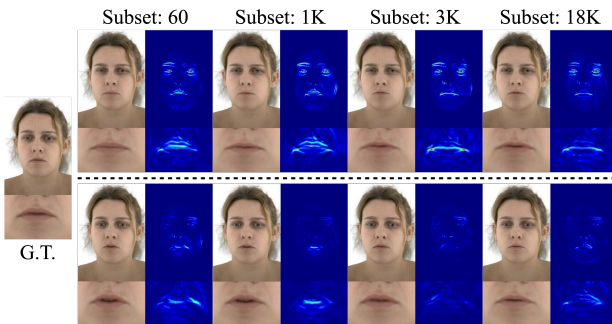


Fig. 6. **Qualitative comparison of GenHMC scalability on UE training.** Training UE with only synthetic data (top) improves performance with more diverse GenHMC subjects, while combining real and synthetic data (bottom) yields robust results. For each case, the UE driving result is on the left, and the L_1 photometric error map (vs. G.T.) is on the right. Colors closer to blue indicate lower error. Kindly refer to our video material for more results.

actually are the pseudo correspondences that the method of Wei et al. [2019] yields for the real HMC captures. As explained in Sec. 5.1.3, this process by itself is prone to bias and errors, which becomes evident when we also train on some real HMC data along with these pseudo labels. In contrast, this encoder is trained with only synthetic HMC images and the actual dome-frame expression latent codes (*i.e.*, perfect ground truth).

For the qualitative evaluations, we also demonstrate a number of frames in the validation set and the corresponding predicted expressions by the aforementioned settings in Fig. 9 (where again, the “G.T.” (ground truth) here is actually the pseudo correspondences). In all cases, the mixed setting (ours) produces the most stable and accurate results. The synthetic-only setting also produces expressive and robust encoding, demonstrating an effective learning of the HMC-avatar correspondences captured by GenHMC.

While we adopted a 50-50 sampling weight for real & synthetic data mix, we note that it is highly likely that a different relative ratio would yield a better outcome, which we leave for future work.

5.3.2 Scaling Law of Number of GenHMC Subjects. Increasing the number of GenHMC training subjects generally leads to decreased photometric L_1 error in the UE training, although this improvement

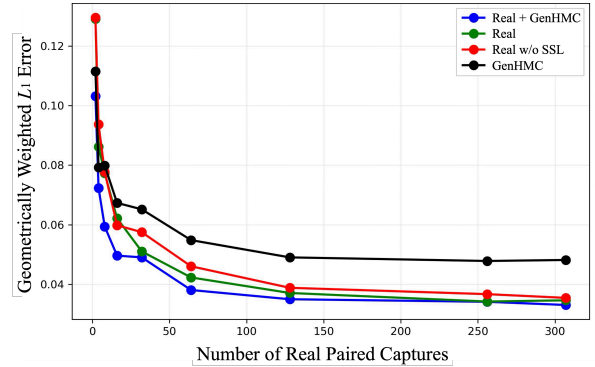


Fig. 7. **Scaling law of number of training subjects (real captures) with UE.** Even with a small number of real training subjects, using synthetic data from GenHMC reliably boosts UE performance. We use all 18K subjects for GenHMC data and report the mean of geometrically weighted L_1 error, which applies spatial importance weighting, emphasizing critical facial regions through UV mapping and predefined weights.

plateaus around 1K to 3K subjects, as shown in Fig. 5. Note that, to isolate the effect of GenHMC data size on encoder performance without the influence of pre-trained priors, we use encoders that are not initialized with SSL pre-trained weights. Also as shown in Fig. 6, while performance improves with more diverse GenHMC training subjects when training solely on synthetic data (top), combining real and GenHMC images (bottom) yields robust UE performance even with GenHMC models trained on as few as 60 subjects.

5.3.3 Scaling Law of Number of Subjects with UE. We investigated the impact of the number of paired captures used to train the downstream UE on its performance. We ablated the number of real captures by training UEs on varying numbers of subjects with maximum of 307 while keeping the number of GenHMC training subjects consistent. As shown in Fig. 7, incorporating synthetic data generated by GenHMC consistently improves UE performance, even with a limited number of real training subjects. This highlights the ability of GenHMC to augment limited real datasets, enhancing the performance and robustness of downstream UE training.

6 Discussion and Conclusions

We introduce GenHMC, a generative approach for synthesizing HMC captures to solve the HMC-avatar correspondence problem in training universal face encoders. Unlike prior analysis-by-synthesis methods, GenHMC improves correspondence quality while removing the need for costly paired captures across camera setups. By training diffusion models conditioned on expression-related features, we enable scalable generation of realistic HMC images. The encoders trained on both real and GenHMC data show improved avatar driving performance and potential for the lower deployment costs, advancing the scalability of photorealistic avatars in VR.

While effective, our method has limitations. It generates frames independently, lacking temporal consistency, and does not condition on subject identity, limiting identity preservation. These issues do not impact on our per-frame, identity-agnostic encoder setup, but addressing these challenges can be a meaningful direction for broader applications.

References

- Hassan Abu Alhaja, Siva Karthik Mustikovela, Lars Mescheder, Andreas Geiger, and Carsten Rother. 2018. Augmented reality meets computer vision: Efficient data generation for urban driving scenes. *International Journal of Computer Vision* 126 (2018), 961–972.
- Shekoofeh Azizi, Simon Kornblith, Chitwan Saharia, Mohammad Norouzi, and David J Fleet. 2023. Synthetic data from diffusion models improves imagenet classification. *arXiv preprint arXiv:2304.08466* (2023).
- Shaojie Bai, Te-Li Wang, Chenghui Li, Akshay Venkatesh, Tomas Simon, Chen Cao, Gabriel Schwartz, Jason Saragih, Yaser Sheikh, and Shih-En Wei. 2024. Universal Facial Encoding of Codec Avatars from VR Headsets. *ACM Trans. Graph.* (2024).
- Yogesh Balaji, Seungjun Nah, Xun Huang, Arash Vahdat, Jiaming Song, Qingsheng Zhang, Karsten Kreis, Miika Aittala, Timo Aila, Samuli Laine, et al. 2022. ediff-i: Text-to-image diffusion models with an ensemble of expert denoisers. *arXiv preprint arXiv:2211.01324* (2022).
- Thabo Beeler, Fabian Hahn, Derek Bradley, Bernd Bickel, Paul A Beardsley, Craig Gotsman, Robert W Sumner, and Markus H Gross. 2011. High-quality passive facial performance capture using anchor frames. *ACM Trans. Graph.* 30, 4 (2011), 75.
- Sai Bi, Stephen Lombardi, Shunsuke Saito, Tomas Simon, Shih-En Wei, Keyvin Mcphail, Ravi Ramamoorthi, Yaser Sheikh, and Jason Saragih. 2021. Deep relightable appearance models for animatable faces. *ACM Transactions on Graphics (ToG)* 40, 4 (2021), 1–15.
- Bernd Bickel, Mario Botsch, Roland Angst, Wojciech Matusik, Miguel Otaduy, Hanspeter Pfister, and Markus Gross. 2007. Multi-scale capture of facial geometry and motion. *ACM transactions on graphics (TOG)* 26, 3 (2007), 33–es.
- Volker Blanz and Thomas Vetter. 1999. A morphable model for the synthesis of 3D faces. In *Proceedings of the 26th annual conference on Computer graphics and interactive techniques*. 187–194.
- Derek Bradley, Wolfgang Heidrich, Tiberiu Popa, and Alla Sheffer. 2010. High resolution passive facial performance capture. In *ACM SIGGRAPH 2010 papers*. 1–10.
- Chen Cao, Tomas Simon, Jin Kyu Kim, Gabe Schwartz, Michael Zollhoefer, Shun-Suke Saito, Stephen Lombardi, Shih-En Wei, Danielle Belko, Shouo-I Yu, Yaser Sheikh, and Jason Saragih. 2022. Authentic volumetric avatars from a phone scan. *ACM Transactions on Graphics (TOG)* 41, 4 (2022), 1–19.
- Chen Cao, Hongzhi Wu, Yanlin Weng, Tianjia Shao, and Kun Zhou. 2016. Real-time facial animation with image-based dynamic avatars. *ACM Transactions on Graphics* 35, 4 (2016).
- Lele Chen, Chen Cao, Fernando De la Torre, Jason Saragih, Chenliang Xu, and Yaser Sheikh. 2021. High-fidelity face tracking for ar/vr via deep lighting adaptation. In *Proceedings of the IEEE/CVF conference on computer vision and pattern recognition*. 13059–13069.
- Yuhua Chen, Wen Li, Xiaoran Chen, and Luc Van Gool. 2019. Learning semantic segmentation from synthetic data: A geometrically guided input-output adaptation approach. In *Proceedings of the IEEE/CVF conference on computer vision and pattern recognition*. 1841–1850.
- Jooyoung Choi, Sungwon Kim, Yonghyun Jeong, Youngjune Gwon, and Sungho Yoon. 2021. llvr: Conditioning method for denoising diffusion probabilistic models. *arXiv preprint arXiv:2108.02938* (2021).
- Timothy F Cootes, Gareth J Edwards, and Christopher J Taylor. 2001. Active Appearance Models. *IEEE Transactions on Pattern Analysis and Machine Intelligence* 23, 6 (2001), 681–685.
- Giannis Daras, Hyungjin Chung, Chieh-Hsin Lai, Yuki Mitsufuji, Jong Chul Ye, Peyman Milanfar, Alexandros G Dimakis, and Mauricio Delbracio. 2024. A survey on diffusion models for inverse problems. *arXiv preprint arXiv:2410.00083* (2024).
- Paul Debevec, Tim Hawkins, Chris Tchou, Haarm-Pieter Duiker, Westley Sarokin, and Mark Sagar. 2000. Acquiring the reflectance field of a human face. In *Proceedings of the 27th annual conference on Computer graphics and interactive techniques*. 145–156.
- Prafulla Dhariwal and Alexander Nichol. 2021. Diffusion models beat gans on image synthesis. *Advances in neural information processing systems* 34 (2021), 8780–8794.
- Craig Donner, Tim Weyrich, Eugene d'Eon, Ravi Ramamoorthi, and Szymon Rusinkiewicz. 2008. A layered, heterogeneous reflectance model for acquiring and rendering human skin. *ACM transactions on graphics (TOG)* 27, 5 (2008), 1–12.
- Philipp Fischer, Alexey Dosovitskiy, Eddy Ilg, Philip Häusser, Caner Hazırbaş, Vladimir Golkov, Patrick Van der Smagt, Daniel Cremers, and Thomas Brox. 2015. FlowNet: Learning optical flow with convolutional networks. *arXiv preprint arXiv:1504.06852* (2015).
- Yasutaka Furukawa and Jean Ponce. 2009. Dense 3d motion capture for human faces. In *2009 IEEE conference on computer vision and pattern recognition*. IEEE, 1674–1681.
- Graham Fyffe, Andrew Jones, Oleg Alexander, Ryosuke Ichikari, and Paul Debevec. 2014. Driving high-resolution facial scans with video performance capture. *ACM Transactions on Graphics (TOG)* 34, 1 (2014), 1–14.
- Baris Gececi, Stylianos Ploumpis, Irene Kotsia, and Stefanos Zafeiriou. 2019. GANFIT: Generative Adversarial Network Fitting for High Fidelity 3D Face Reconstruction. In *Proceedings of the IEEE/CVF Conference on Computer Vision and Pattern Recognition (CVPR)*.
- Abhijeet Ghosh, Graham Fyffe, Borom Tunwattanapong, Jay Busch, Xueming Yu, and Paul Debevec. 2011. Multiview face capture using polarized spherical gradient illumination. In *Proceedings of the 2011 SIGGRAPH Asia Conference*. 1–10.
- Philip-William Grassal, Malte Prinzler, Titus Leistner, Carsten Rother, Matthias Nießner, and Justus Thies. 2022. Neural head avatars from monocular rgb videos. In *Proceedings of the IEEE/CVF Conference on Computer Vision and Pattern Recognition*. 18653–18664.
- Ruifei He, Shuyang Sun, Xin Yu, Chuhui Xue, Wenqing Zhang, Philip Torr, Song Bai, and XIAOJUAN QI. 2023. IS SYNTHETIC DATA FROM GENERATIVE MODELS READY FOR IMAGE RECOGNITION?. In *The Eleventh International Conference on Learning Representations*.
- Amir Hertz, Ron Mokady, Jay Tenenbaum, Kfir Aberman, Yael Pritch, and Daniel Cohen-Or. 2022. Prompt-to-prompt image editing with cross attention control. *arXiv preprint arXiv:2208.01626* (2022).
- Jonathan Ho, Ajay Jain, and Pieter Abbeel. 2020. Denoising diffusion probabilistic models. *Advances in neural information processing systems* 33 (2020), 6840–6851.
- Jonathan Ho and Tim Salimans. 2022. Classifier-free diffusion guidance. *arXiv preprint arXiv:2207.12598* (2022).
- Andrew Howard, Mark Sandler, Grace Chu, Liang-Chieh Chen, Bo Chen, Mingxing Tan, Weijun Wang, Yukun Zhu, Ruoming Pang, Vijay Vasudevan, et al. 2019. Searching for mobilenetv3. In *Proceedings of the IEEE/CVF international conference on computer vision*. 1314–1324.
- Li Hu. 2024. Animate anyone: Consistent and controllable image-to-video synthesis for character animation. In *Proceedings of the IEEE/CVF Conference on Computer Vision and Pattern Recognition*. 8153–8163.
- Jin Huang, Xiaohan Shi, Xinguo Liu, Kun Zhou, Li-Yi Wei, Shang-Hua Teng, Hujun Bao, Baining Guo, and Heung-Yeung Shum. 2006. Subspace gradient domain mesh deformation. In *ACM SIGGRAPH 2006 Papers*. 1126–1134.
- Alexandru Eugen Ichim, Sofien Bouaziz, and Mark Pauly. 2015. Dynamic 3D avatar creation from hand-held video input. *ACM Transactions on Graphics (ToG)* 34, 4 (2015), 1–14.
- Bahjat Kawar, Shiran Zada, Oran Lang, Omer Tov, Huiwen Chang, Tali Dekel, Inbar Mosseri, and Michal Irani. 2023. Imagic: Text-based real image editing with diffusion models. In *Proceedings of the IEEE/CVF Conference on Computer Vision and Pattern Recognition*. 6007–6017.
- Martin Klaudiny and Adrian Hilton. 2012. High-detail 3D capture and non-sequential alignment of facial performance. In *2012 Second International Conference on 3D Imaging, Modeling, Processing, Visualization & Transmission*. IEEE, 17–24.
- Hao Li, Laura Trutou, Kyle Olszewski, Lingyu Wei, Tristan Trutna, Pei-Lun Hsieh, Aaron Nicholls, and Chongyang Ma. 2015. Facial Performance Sensing Head-mounted Display. *ACM Transactions on Graphics (TOG)* 34, 4, Article 47 (July 2015), 47:1–47:9 pages.
- Junxuan Li, Chen Cao, Gabriel Schwartz, Rawal Khirodkar, Christian Richardt, Tomas Simon, Yaser Sheikh, and Shunsuke Saito. 2024. URAvatar: Universal Relightable Gaussian Codec Avatars. In *ACM SIGGRAPH Asia 2024 Conference Papers*.
- Luping Liu, Yi Ren, Zhijie Lin, and Zhou Zhao. 2022. Pseudo numerical methods for diffusion models on manifolds. *arXiv preprint arXiv:2202.09778* (2022).
- Stephen Lombardi, Jason Saragih, Tomas Simon, and Yaser Sheikh. 2018. Deep appearance models for face rendering. *ACM Transactions on Graphics (ToG)* 37, 4 (2018), 1–13.
- Cheng Lu, Yuhao Zhou, Fan Bao, Jianfei Chen, Chongxuan Li, and Jun Zhu. 2022. Dpm-solver: A fast ode solver for diffusion probabilistic model sampling in around 10 steps. *Advances in Neural Information Processing Systems* 35 (2022), 5775–5787.
- Julietta Martinez, Emily Kim, Javier Romero, Timur Bagautdinov, Shunsuke Saito, Shouo-I Yu, Stuart Anderson, Michael Zollhoefer, Te-Li Wang, Shaojie Bai, et al. 2024. Codec Avatar Studio: Paired Human Captures for Complete, Driveable, and Generalizable Avatars. In *The Thirty-eight Conference on Neural Information Processing Systems Datasets and Benchmarks Track*.
- Nikolaus Mayer, Eddy Ilg, Philip Häusser, Philipp Fischer, Daniel Cremers, Alexey Dosovitskiy, and Thomas Brox. 2016. A large dataset to train convolutional networks for disparity, optical flow, and scene flow estimation. In *Proceedings of the IEEE conference on computer vision and pattern recognition*. 4040–4048.
- Vinod Nair, Josh Susskind, and Geoffrey E. Hinton. 2008. Analysis-by-Synthesis by Learning to Invert Generative Black Boxes. In *Proceedings of the 18th International Conference on Artificial Neural Networks (ICANN), Part I* (Prague, Czech Republic). 971–981.
- Alexander Quinn Nichol, Prafulla Dhariwal, Aditya Ramesh, Pranav Shyam, Pamela Mishkin, Bob McGrew, Ilya Sutskever, and Mark Chen. 2022. GLIDE: Towards Photorealistic Image Generation and Editing with Text-Guided Diffusion Models. In *International Conference on Machine Learning*. PMLR, 16784–16804.
- Kyle Olszewski, Joseph J. Lim, Shunsuke Saito, and Hao Li. 2016. High-fidelity Facial and Speech Animation for VR HMDs. *ACM Transactions on Graphics (TOG)* 35, 6, Article 221 (Nov. 2016), 14 pages.
- Xingchao Peng, Baochen Sun, Karim Ali, and Kate Saenko. 2015. Learning deep object detectors from 3d models. In *Proceedings of the IEEE international conference on computer vision*. 1278–1286.

- Angus Phillips, Hai-Dang Dau, Michael John Hutchinson, Valentin De Bortoli, George Deligiannidis, and Arnaud Doucet. 2024. Particle Denoising Diffusion Sampler. *arXiv preprint arXiv:2402.06320* (2024).
- Aditya Ramesh, Prafulla Dhariwal, Alex Nichol, Casey Chu, and Mark Chen. 2022. Hierarchical text-conditional image generation with clip latents. *arXiv preprint arXiv:2204.06125* 1, 2 (2022), 3.
- Robin Rombach, Andreas Blattmann, Dominik Lorenz, Patrick Esser, and Björn Ommer. 2022. High-resolution image synthesis with latent diffusion models. In *Proceedings of the IEEE/CVF conference on computer vision and pattern recognition*. 10684–10695.
- German Ros, Laura Sellart, Joanna Materzynska, David Vazquez, and Antonio M Lopez. 2016. The synthia dataset: A large collection of synthetic images for semantic segmentation of urban scenes. In *Proceedings of the IEEE conference on computer vision and pattern recognition*. 3234–3243.
- Radu Alexandru Rosu, Shunsuke Saito, Ziyang Wang, Chenglei Wu, Sven Behnke, and Giljoo Nam. 2022. Neural strands: Learning hair geometry and appearance from multi-view images. In *European Conference on Computer Vision*. Springer, 73–89.
- Chitwan Saharia, William Chan, Saurabh Saxena, Lala Li, Jay Whang, Emily L Denton, Kamyar Ghasemipour, Raphael Gontijo Lopes, Burcu Karagol Ayan, Tim Salimans, et al. 2022. Photorealistic text-to-image diffusion models with deep language understanding. *Advances in neural information processing systems* 35 (2022), 36479–36494.
- Mert Bülent Saryıldız, Kartek Alahari, Diane Larlus, and Yannis Kalantidis. 2023. Fake it till you make it: Learning transferable representations from synthetic imagenet clones. In *Proceedings of the IEEE/CVF Conference on Computer Vision and Pattern Recognition*. 8011–8021.
- Gabriel Schwartz, Shih-En Wei, Te-Li Wang, Stephen Lombardi, Tomas Simon, Jason Saragih, and Yaser Sheikh. 2020. The eyes have it: An integrated eye and face model for photorealistic facial animation. *ACM Transactions on Graphics (TOG)* 39, 4 (2020), 91–1.
- Mike Seymour, Chris Evans, and Kim Libreri. 2017. Meet mike: epic avatars. In *ACM SIGGRAPH 2017 VR Village*. 1–2.
- Yichun Shi, Peng Wang, Jianglong Ye, Mai Long, Kejie Li, and Xiao Yang. 2023. Mvdream: Multi-view diffusion for 3d generation. *arXiv preprint arXiv:2308.16512* (2023).
- Aliaksandra Shysheya, Egor Zakharov, Kara-Ali Aliev, Renat Bashirov, Egor Burkov, Karim Iskakov, Aleksei Ivakhnenko, Yury Malkov, Igor Pasechnik, Dmitry Ulyanov, Alexander Vakhitov, and Victor Lempitsky. 2019. Textured Neural Avatars. In *Proceedings of the IEEE/CVF Conference on Computer Vision and Pattern Recognition (CVPR)*.
- Jascha Sohl-Dickstein, Eric Weiss, Niru Maheswaranathan, and Surya Ganguli. 2015. Deep unsupervised learning using nonequilibrium thermodynamics. In *International conference on machine learning*. PMLR, 2256–2265.
- Jiaming Song, Chenlin Meng, and Stefano Ermon. 2020a. Denoising Diffusion Implicit Models. In *International Conference on Learning Representations*.
- Yang Song and Stefano Ermon. 2019. Generative modeling by estimating gradients of the data distribution. *Advances in neural information processing systems* 32 (2019).
- Yang Song, Liyue Shen, Lei Xing, and Stefano Ermon. 2021. Solving inverse problems in medical imaging with score-based generative models. *arXiv preprint arXiv:2111.08005* (2021).
- Yang Song, Jascha Sohl-Dickstein, Diederik P Kingma, Abhishek Kumar, Stefano Ermon, and Ben Poole. 2020b. Score-based generative modeling through stochastic differential equations. *arXiv preprint arXiv:2011.13456* (2020).
- Justus Thies, Michael Zollhöfer, Marc Stamminger, Christian Theobalt, and Matthias Niessner. 2018. FaceVR: Real-Time Gaze-Aware Facial Reenactment in Virtual Reality. *ACM Transactions on Graphics (TOG)* 37, 2, Article 25 (June 2018), 25:1–25:15 pages.
- Yonglong Tian, Lijie Fan, Phillip Isola, Huiwen Chang, and Dilip Krishnan. 2024. Stablerep: Synthetic images from text-to-image models make strong visual representation learners. *Advances in Neural Information Processing Systems* 36 (2024).
- Brandon Trabucco, Kyle Doherty, Max Gurinas, and Ruslan Salakhutdinov. 2023. Effective data augmentation with diffusion models. *arXiv preprint arXiv:2302.07944* (2023).
- Daniel Watson, William Chan, Jonathan Ho, and Mohammad Norouzi. 2022. Learning fast samplers for diffusion models by differentiating through sample quality. In *International Conference on Learning Representations*.
- Shih-En Wei, Jason Saragih, Tomas Simon, Adam W. Harley, Stephen Lombardi, Michal Perdoch, Alexander Hypes, Dawei Wang, Hernan Badino, and Yaser Sheikh. 2019. VR Facial Animation via Multiview Image Translation. *ACM Trans. Graph.* (2019).
- Tim Weyrich, Wojciech Matusik, Hanspeter Pfister, Bernd Bickel, Craig Donner, Chien Tu, Janet McAndless, Jinho Lee, Addy Ngan, Henrik Wann Jensen, et al. 2006. Analysis of human faces using a measurement-based skin reflectance model. *ACM Transactions on Graphics (ToG)* 25, 3 (2006), 1013–1024.
- Haotian Yang, Mingwu Zheng, Wanquan Feng, Haibin Huang, Yu-Kun Lai, Pengfei Wan, Zhongyuan Wang, and Chongyang Ma. 2023. Towards practical capture of high-fidelity relightable avatars. In *SIGGRAPH Asia 2023 Conference Papers*. 1–11.
- Lvmin Zhang, Anyi Rao, and Maneesh Agrawala. 2023. Adding conditional control to text-to-image diffusion models. In *Proceedings of the IEEE/CVF International Conference on Computer Vision*. 3836–3847.
- Li Zhang, Noah Snavely, Brian Curless, and Steven M Seitz. 2004. Spacetime faces: high resolution capture for modeling and animation. In *ACM SIGGRAPH 2004 Papers*. 548–558.
- Yi Zhou, Connelly Barnes, Jingwan Lu, Jimei Yang, and Hao Li. 2019. On the continuity of rotation representations in neural networks. In *Proceedings of the IEEE/CVF conference on computer vision and pattern recognition*. 5745–5753.

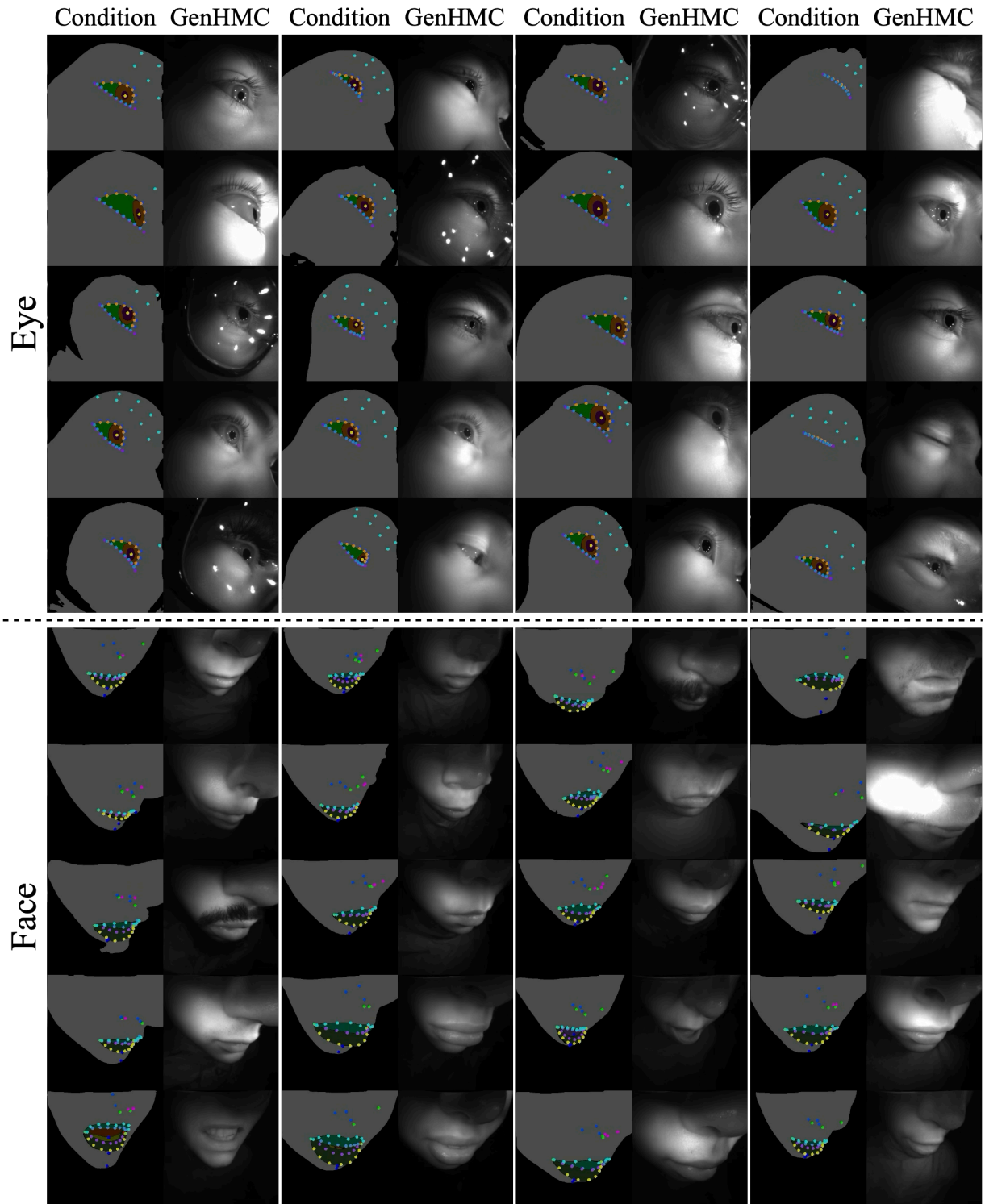


Fig. 8. **Qualitative results of GenHMC.** Using a keyseg map as a condition (the left image in each group), our GenHMC generates synthetic HMC images (right) that feature diverse natural augmentations for a single expression.

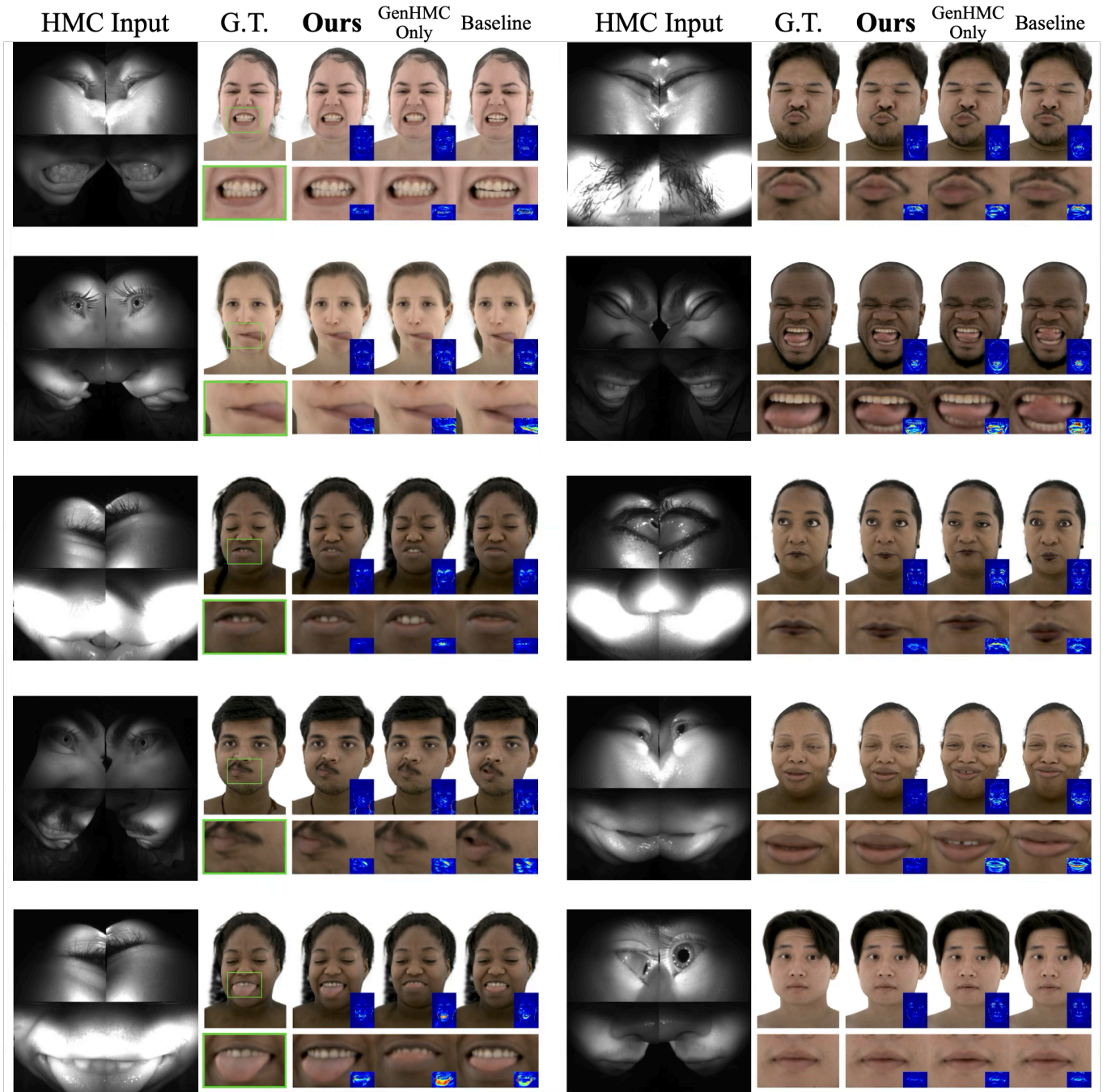


Fig. 9. **Qualitative Comparisons of Universal Encoder (UE).** We present a qualitative comparison of encoders trained with real data and/or GenHMC synthetic data under 3 configurations. For each column, the images are from left to right: HMC input images, ground truth rendering, **Ours (50% Real-50% Synthetic)**, **GenHMC (Synthetic) Only**, and **Baseline (Real Only)** [Bai et al. 2024]. The error map of each encoder’s prediction with respect to the ground truth is shown in the bottom-right corner of each rendering. Our results indicate that the mixed real–synthetic training strategy effectively improves inner mouth tracking, capturing subtleties such as tongue movements and teeth closure.

Generative Head-Mounted Camera Captures for Photorealistic Avatars

Supplementary Material

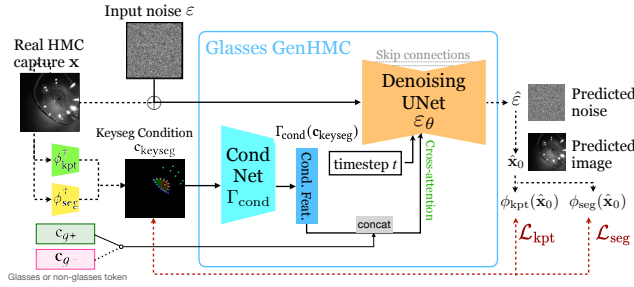


Fig. A. **Glasses GenHMC training framework.** From Fig. 2, we introduce an additional glasses encoding token $c_{g\pm}$ corresponding to whether the training sample has glasses or not, concatenated to the keypoint-segmentation condition tokens. At inference time, we can choose to set this token to either c_{g+} or c_{g-} to optionally generate glasses in the eye HMCs. Some losses from Fig. 2 are omitted for brevity.

We also explore various applications of GenHMC, leading to more controllable framework. First, Sec. A explores augmentations involving accessories like glasses, enabling the generation of synthetic HMC captures for a wider range of appearances. Second, as detailed in Sec. B, we improve the consistency of synthetic subjects across the different views by leveraging the 3D self-attention mechanism used in multi-view diffusion frameworks and incorporating camera parameters into the diffusion model through timestep embeddings. Finally, we incorporate light source maps as additional conditional inputs as well as keyseg maps, enabling controllable lighting augmentations (Sec. C).

A Glasses Control

Wearing glasses under the VR headset device is a common use case, and therefore we want to collect data representing this distribution. However, collecting usable HMC data with subjects wearing glasses is a challenge in itself, and the presence of glasses (and LED reflections on the lenses) also significantly interferes with the person-specific style transfer module that the traditional method of Wei et al. [2019] needed to establish HMC-avatar correspondences. Therefore, the traditional approach could not handle glasses cases well, frequently generating inaccurate “ground truth” expression codes for the downstream encoder training usage.

In contrast, GenHMC provides an easy solution to this. Specifically, we can extend the regular GenHMC in Sec. 4.1 to be additionally *glasses-conditional*, i.e., **Glasses GenHMC**, where we generate a synthetic HMC dataset with glasses that comes with accurate, dome-frame ground truth expression codes, provided an initial volume of unpaired HMC captures with and without glasses.

To achieve this, we take advantage of a large, unpaired (with dome captures) collection of HMC captures, where frames in the dataset are tagged with binary labels of glasses on or off for each particular capture, $\{g+, g-\}$ (this can be done in an automated way

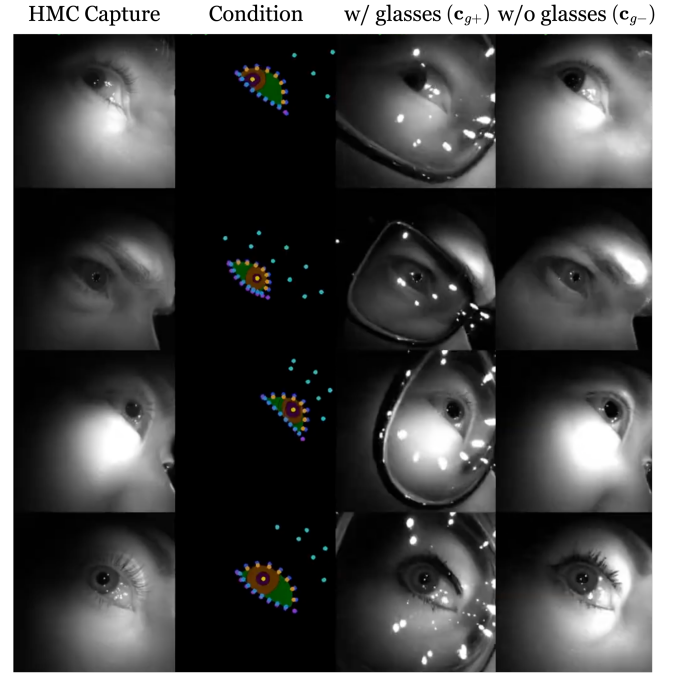


Fig. B. **Qualitative results of Glasses GenHMC.** Left to right: reference raw HMC image, detected keypoint-segmentation conditional, diffusion with glasses, diffusion without glasses. Note that the segmentation map of facial area is not used for Glasses GenHMC to prevent “cheating”, which could bias the training process towards the semantic leakage of the conditional.

by training a binary classifier as well). The diffusion model is then trained as described before in Sec. 4.1 with the same losses, but the conditional is now a concatenation of the corresponding glasses embedding token $\{c_{g+}, c_{g-}\} \in \mathbb{R}^C$ (e.g., $C = 160$ as in Sec. 4.1) and the flattened feature map $\Gamma_{\text{cond}}(c)$ for every sample, as illustrated in Fig. A. In this way, the model learns conditioning context from not only the keyseg map informing sparse facial structure, but also a controllable binary token we insert indicating glasses presence. Fig. B shows that we can successfully generate synthetic HMC data with glasses (c_{g+}), while following the same keyseg map as those without glasses (c_{g-}).

B Multi-view Consistency

For a single subject, HMC captures are collected from multiple different camera views. However, regular GenHMC uses the detected keyseg map corresponding to a single view as a condition to generate synthetic outputs, which does not guarantee consistency across different views.

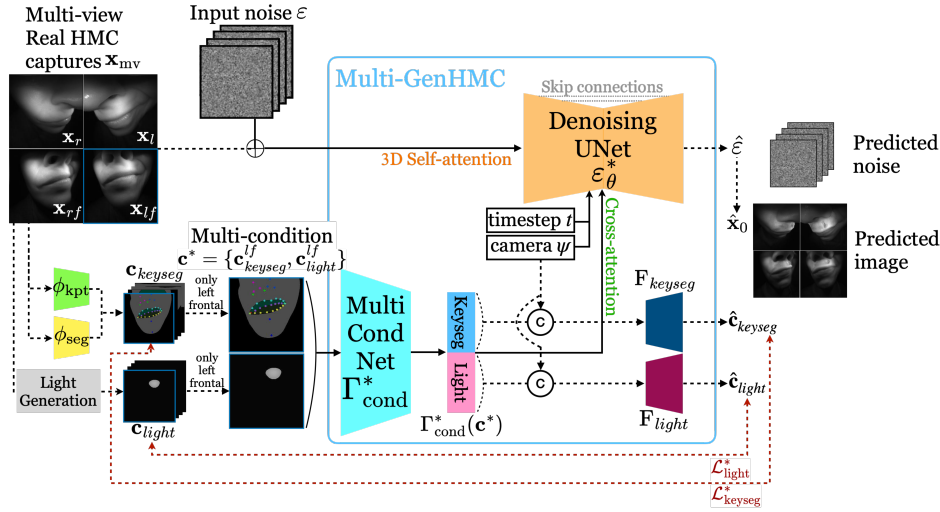


Fig. C. **Multi-GenHMC training framework.** We leverage the light source map as an additional condition to achieve more precise control over illuminance, and generate multi-view consistent HMC captures by using the camera parameters and 3D self-attention. Note that the training objectives used in regular GenHMC have been omitted for simplicity in the figure.

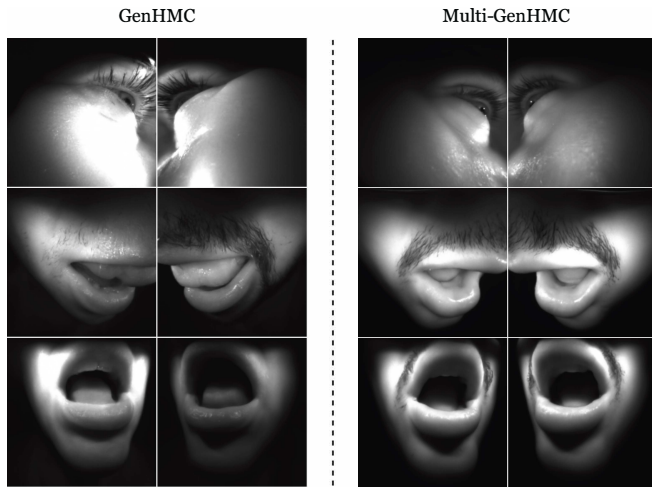


Fig. D. **Synthetic HMC image examples of GenHMC and Multi-GenHMC.** While GenHMC generates synthetic HMC captures per view and may exhibit different facial details across different views even within the same frame, Multi-GenHMC ensures consistent details for the target views during generation.

To address this point, we further conceptualize **Multi-GenHMC**, which leverages multi-view real HMC data and their camera parameters to generate synthetic captures that consistently share details across different views, as illustrated in Fig. C. Inspired by [Shi et al. 2023], a multi-view diffusion framework capable of generating 3D-consistent outputs, we utilize camera parameters and 3D self-attention to produce multi-view consistent synthetic captures. Given multi-view real HMC captures $\mathbf{x}_{mv} = \{\mathbf{x}_r, \mathbf{x}_l, \mathbf{x}_{rf}, \mathbf{x}_{lf}\}$ consisting of right, left, right-frontal, and left-frontal views, and 12-dimensional

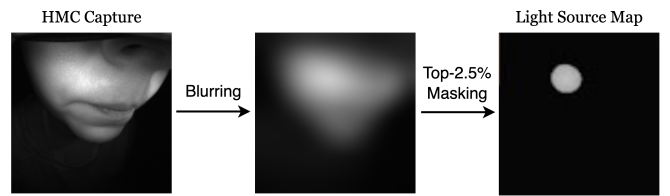


Fig. E. **Light source map generation.** A light source map, which serves as a conditional signal for lighting, is generated from the input real HMC capture through the blurring and top-value masking process.

camera parameters ψ (comprising 6D rotation [Zhou et al. 2019] and camera intrinsic parameters), the camera parameters ψ , which are embedded together with timestep t , are processed through U-Net \mathcal{E}_θ^* equipped with 3D self-attention. As shown in Fig. D, the details of the generated images, e.g., mustache, tongue position, and eye-lashes, are much more consistent across different views compared to regular GenHMC. Note that \mathcal{E}_θ^* is trained with the same training losses as regular GenHMC.

C Light Control

Another interesting extension of the GenHMC framework is flexible control over the LED illuminations for the synthetic capture. Based on Multi-GenHMC, we incorporate our proposed light source map described in Fig. E as an additional condition \mathbf{c}_{light} , alongside the existing keyseg map \mathbf{c}_{keyseg} .

First, the light source map is generated during training by applying a Gaussian kernel to blur the target HMC capture. This process removes identity-specific details while retaining abstract illumination-related information. Afterward, we retain only the top 2.5% of values from the blurred HMC image, corresponding to areas where light intensity is the strongest, to create a point-like

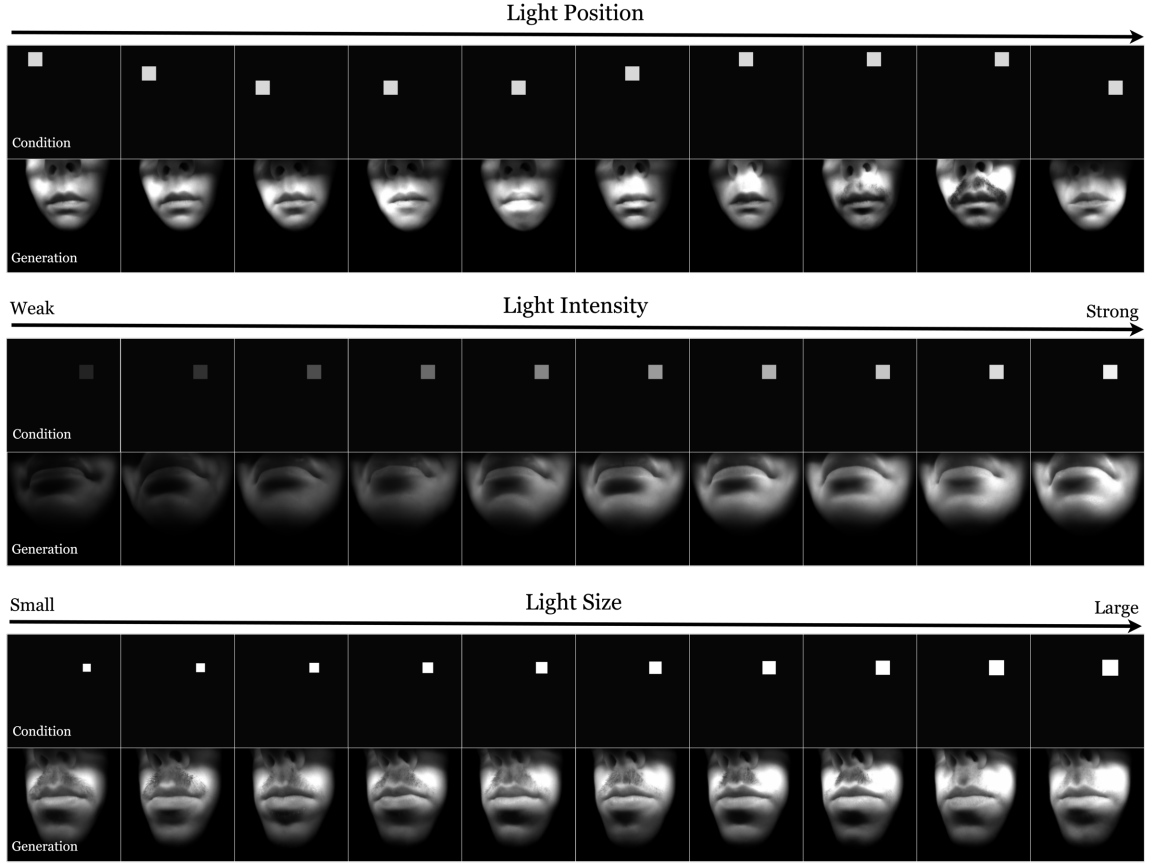


Fig. F. **Light control with arbitrary light source maps.** With our proposed framework, we can generate synthetic HMC images following diverse illuminance conditions, *e.g.*, light position, intensity, and size. Note that the identical keyseg maps are used for each row.

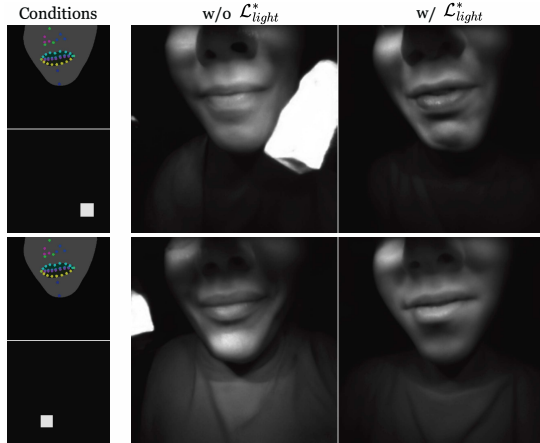


Fig. G. **Effect of the proposed light reconstruction loss \mathcal{L}_{light}^* .** Without \mathcal{L}_{light}^* , more artifacts occur on the background during inference when given the uncommon light conditions, *e.g.*, the light source positioned outside the facial region.

representation serving as the final light source map. By using our proposed light source map as a condition, the model captures the illumination information of the target HMC capture. The additional light condition allows for finer control over not only the expressions tied to the keyseg map but also the illumination of synthetic HMC captures, providing more flexibility in augmentation. As illustrated in Fig. F, we are able to generate synthetic data with fine controls on light condition.

Furthermore, in a multi-view framework where synthesized views are adjusted based on camera parameters ψ , training with all conditions corresponding to each viewpoint can lead to entanglement between the generated image’s viewpoint and other conditional inputs. To prevent this, we set the left-frontal view as the reference view and use only its keyseg map and light source map as input conditions $\mathbf{c}^* = \{\mathbf{c}_{keyseg}^{lf}, \mathbf{c}_{light}^{lf}\}$. Additionally, we introduce additional networks F_{keyseg} and F_{light} , which take the first and the other half of the conditional feature vector $\Gamma_{cond}^*(\mathbf{c}^*) \in \mathbb{R}^{C \times 64}$ that are processed from \mathbf{c}_{keyseg} and \mathbf{c}_{light} , respectively, and camera parameters ψ as inputs and are trained to reconstruct the original conditional

inputs for all the target views, including left-frontal:

$$\mathcal{L}_{keyseg}^* = \|\hat{\mathbf{c}}_{keyseg} - \mathbf{c}_{keyseg}\|_2^2, \quad (8)$$

$$\mathcal{L}_{light}^* = \|\hat{\mathbf{c}}_{light} - \mathbf{c}_{light}\|_2^2, \quad (9)$$

leading to improved quality of the generated outputs dependent on their conditions, e.g., Fig. G shows the improved output with effectively reduced background artifacts when given unusual \mathbf{c}_{light} .

Inference largely follows the same process as regular GenHMC, except that it uses left-frontal avatar rendering to extract keyseg map, camera parameters, and the light source map as additional conditions. It ensures consistent synthetic outputs while maintaining flexibility in lighting and view conditions.

Received 20 February 2007; revised 12 March 2009; accepted 5 June 2009